Different enrichment patterns of magnetic particles modulated by primary iron-phosphorous input

Juan Ren[1], Xiaoyong Long[1*], Junfeng Ji[2], Vidal Barrón[3], José Torrent[3], Yong Wang[1], Shiyou Xie[1]

[1]School of Geographical Sciences, Southwest University, Chongqing, China

[2]Institute of Surficial Geochemistry, College of Earth Sciences and Engineering, Nanjing University, Nanjing, China

[3]Departamento de Agronomía, Universidad de Córdoba, Córdoba, Spain

*Corresponding author: Xiaoyong Long (longxy@126.com);

Key Points:

- Iron oxide crystallinity increases monotonically as soil P/Fe decreases
- Ferrimagnets accompanying the formation of hematite are enriched with accelerations under high P/Fe but with even rates under low P/Fe
- Ferrimagnets grow and transform into hematite more rapidly without the proper level of P ligand protection

Abstract

Magnetic particles associated with iron (Fe) oxides are widespread on the surface of Earth and Mars and serve as reasonable climatic indicators. Ferrimagnetic maghemite (Mgh) and antiferromagnetic hematite (Hm), which dominate magnetism and redness, often coexist or compete with each other in soils and sediments. The formation efficiency of Mgh relative to Hm could be modulated by geochemical background in addition to climate, especially by phosphate (P), which has a high affinity on the surface of precursor iron oxides in natural systems. We investigated two Ferralsol sequences around a P mining field with comparable climate but contrasting P/Fe ratios. High P/Fe retards iron oxide crystallization as well as grain growth and transformation into Hm, which thereby promotes more effective accumulation of ferrimagnetic Mgh as intermediate products. The ligand-protected effect well interprets asynchronous changes in magnetism and redness in soils and sediments across large spatial and temporal scales.

Plain Language Summary

Iron (Fe) oxides are critical carriers of magnetism and dyeing agents of color in soils and sediments. Magnetic properties and color indices are widely employed in soil taxonomy, paleoclimate reconstruction and spatial exploration. However, the maghemite (Mgh) and hematite (Hm) dominating magnetism and redness often coexist or compete with each other in natural systems. The process depends on climatic conditions and geochemical background; however, the two effects are often mixed. Phosphorous (P) derived from parent materials usually demonstrates obvious

differences, and phosphate is considered the most important ligand affecting the formation of precursor iron oxides in natural systems. To explore the independent effect of P/Fe on the formation efficiency of Hm and Mgh, we investigated two Ferralsol profile sequences around a P mining field with similar climates but different P/Fe ratios. High P/Fe impedes iron oxide crystallization as well as grain growth and transformation into Hm, which thereby promotes more effective accumulation of ferrimagnetic Mgh as an intermediate product. This lack of ligand-protected effects would help interpret asynchronous changes in magnetism and color in soils and sediments across large spatial and temporal scales, especially in red soils and sediments with a high intensity of chemical weathering.

1 Introduction

Magnetic particles associated with pedogenic iron (Fe) oxides are ubiquitous on the surface of Earth and Mars as the preferential weathering product of Fe-bearing minerals [*Christensen et al., 2001*]. Magnetic particles can be divided into ferrimagnetic (FM) and antiferromagnetic (AFM) particles according to magnetic properties. The FM particles, mainly maghemite (Mgh, γ-Fe_2O_3) and magnetite (Mgt, Fe_3O_4), often dominate magnetism, although they contribute a low weight to the total amount of iron oxides in soils and sediments [*Liu et al., 2012*]. On the other hand, AFM particles include hematite (Hm, α-Fe_2O_3) and goethite (Gt, α-FeOOH), which are the main red and yellow color agents, respectively, in soils and sediments [*Davey et al., 1975*].

In past decades, the magnetic properties determined by the content and ratio of FM particles with differing sizes have widely been employed as pedogenic indicators in soil taxonomy and paleoclimate reconstruction, especially in the aeolian sediments of Quaternary loess and Tertiary red clay deposited on the Chinese Loess Plateau (CLP) [*Mullins, 1977; Liu et al., 2003; Maher, 2011; Maxbauer et al., 2016; Nie et al., 2016*]. Meanwhile, the color indices and spectral characteristics mainly determined by AFM Hm and Gt have been extensively used in soil taxonomy [*Mullins, 1977*] and paleoclimate reconstruction [*Deng et al., 2006; Liu et al., 2006; Torrent et al., 2006; Chen et al., 2010*]. Moreover, the ratios of Hm and Gt, which directly reflect the soil moisture and relative humidity of the regional climate [*Cornell and Schwtermann, 2003*], prove to be helpful in the interpretation of nonlinear magnetic responses to

climate in soils and sediments [*Xiong and Li, 1987; Balsam et al., 2004; Ji et al., 2004; Liu et al., 2006; Torrent et al., 2006; Nie et al., 2010; Liu et al., 2013; Long et al., 2016; Gao et al., 2018*].

To date, the formation mechanisms of FM and AFM particles with pedogenesis are still under debate due to field works and laboratory syntheses conducted under wide climate ranges and variable conditions [*Lovley and Phillips, 1986; Gálvez et al., 1999; Barrón and Torrent, 2002; Liu et al., 2003*]. Nevertheless, the genetic relation between the small amount of FM particles and AFM particles has gradually been confirmed by growing evidence [*Torrent et al., 2006; Long et al., 2015, 2016*], especially after Mgh-like particles with increasing size from superparamagnetic (SP) to single domain (SD) were found to act as intermediate products of Hm in solution under ambient conditions [*Barrón and Torrent, 2002; Liu et al., 2008; Gutiérrez et al., 2016; Jiang et al., 2018*]. These experiments demonstrate the common positive correlation between magnetism and redness at a large scale [*Torrent et al., 2006; Long et al., 2015, 2016*]. However, the relative formation efficiency of Mgh and Hm seems to be modulated by the water activity [*Long et al., 2016*] and ligand adsorption of precursor iron oxides [*Cabello et al., 2009*] due to the similar thermodynamic stability of Mgh and Hm in nanometers [*Chernyshova et al., 2007; Navrotsky et al., 2008; Hiemstra, 2015*]. Our previous study found significant grain growth of Mgh particles and their transformation to Hm in tropical Ferralsol, with a high formation efficiency estimated by an Hm/(Hm+Gt) above 0.6 [*Long et al., 2015*]. However, in some red soil formed in subtropical and tropical regions or red strata formed from the Mesozoic

to Cenozoic, the lower magnetism is out of phase with higher redness [*Han et al., 1996; Yang et al., 2001; Nie et al., 2010; Hu et al., 2014; Nie et al., 2016*], although the Hm/(Hm+Gt) values are mostly below 0.6, and the positive correlation between redness and magnetism is still maintained in these soils and sediments [*Liu et al., 2006; Torrent et al., 2006*]. Considering that these soils and sediments have commonly undergone more chemical weathering under the warm climate [*Guo et al., 2002; Fang et al., 2003*], the weathering intensity accompanied by the lack of ligands could change the relative formation efficiency of Mgh and Hm, in addition to climate, at a large scale.

Various organic and inorganic ligands have been introduced as additives to modulate the phase and size of the aging product of precursor iron oxides in laboratory experiments [*Gálvez et al., 1999; Barrón and Torrent, 2002; Cabello et al., 2009; Wang et al., 2017; Xu et al., 2017; Jiang et al., 2018; Wang et al., 2018*], especially phosphate (P) because of the high affinity for iron (Fe) oxides *[Gálvez et al., 1999; Barrón and Torrent, 2002]*. In natural systems, the phosphate derived from different parent materials varies greatly [*Ruttenberg, 2003*], and the P/Fe often exhibits significant change with chemical weathering since the primary P tends to be leached, while the primary Fe tends to be enriched in soils and sediments [*Taylor and Schwertmann, 1974*]. The P absorbed and occluded by different iron oxides has been widely discussed in subtropical and tropical soils [*Borggaard, 1983; Chacon et al., 2006; Vilar et al., 2010; Bortoluzzi et al., 2015; Fink et al., 2016; Zhao et al., 2018; Brenner et al., 2019; Poggere et al., 2020*], whereas the effect of P on the formation

of pedogenic iron oxides has been partly ignored because the effect is mostly mixed with climate. To explore the independent effect of P/Fe on the formation efficiency of Mgh and Hm in natural systems, we focused on two Ferralosl sequences around a P mining area with a similar climate but contrasting ratio of P/Fe. This approach provides us with an opportunity to evaluate the independent influence of phosphate ligands on the formation efficiency of various magnetic particles in natural systems and interpret the asynchronous changes in magnetism and redness in soils and sediments at large spatial and temporal scales.

2 Materials and Methods

The two soil sequences were sampled around the Kunyang P mining area, which is located on the Yunnan Plateau in southwestern China and is one of the largest P mining areas in the world. This mining area is derived from Paleozoic siliceous dolomite strata that contain phosphorite with a P_2O_5 proportion as high as 36% [*Xiao et al., 2019*]. The mean altitude of the Yunnan Plateau is approximately 2000 m, and the climate is relatively dry and warm, with a mean annual precipitation of 994 mm and a mean annual temperature of 15.1°C. All profiles were sampled on a highland with well drainage on both sides of a valley across the area. The uppermost soils can be categorized as Ferralsol, which were considered to have undergone strong chemical weathering since the uplift of the Yunnan Plateau in the Late Cenozoic [*Yin, 2010*]. The profiles were covered by natural woodlands and grasslands. The soil samples were collected from the surface to the bottom of outcrops at intervals of 20 cm or 40 cm depending on the thickness of the profile.

The air-dried soil samples were sieved to < 2 mm and ground into powders to conduct chemical analysis. The chemical compositions were determined by the X-ray fluorescence method using ARL9800XP + XRF spectrometry. The chemical index of alteration (CIA) was calculated as $Al_2O_3/(Al_2O_3 + CaO + Na_2O + K_2O)$ by the molar ratio. The P/Fe was calculated by the molar ratio of P_2O_5 and Fe_2O_3. The total Fe (Fe_t) and total P (P_t) were also calculated from the contents of Fe_2O_3 and P_2O_5. Free iron (Fe_d) and amorphous iron (Fe_o) were extracted with citrate-bicarbonate-dithionite (CBD) and ammonium oxalate, respectively. Diffuse reflectance spectra (DRS) were measured on a Perkin-Elimer Lambda 900 spectrophotometer at 2-nm intervals. The redness was calculated as the ratio of the average reflectance in the red light band (630 ~ 700 nm) and visual light band (400 ~ 700 nm). The standard Hm and Gt minerals used in the experiment were Pfizer R1599 red and Hoover Color Corporation Synox Hy610 yellow. The Hm was estimated by a working curve established by the deferrated samples mixed with a series of given contents of standard Hm and Gt according to the procedure in our previous study [*Long et al., 2011*]. Finally, the Hm and Gt contents were calculated by the following equations when we assign free iron oxides (Fe_d) to the combination of iron in stoichiometric Hm (Fe_2O_3), Gt (FeOOH) [*Torrent et al., 2007*] and Fe_o:

$$\text{Hm (\%)} = 10^{-4} \times e^{23.03 * \text{Redness}}$$

$$\text{Gt (\%)} = 1.59 \times (Fe_d - Fe_o - \text{Hm}/1.43)$$

Magnetic susceptibility (χ) was measured with an MS2 instrument from Bartington. The low-frequency (χ_{lf}) and high-frequency (χ_{hf}) values were determined

at 0.47 and 4.7 kHz, respectively, to estimate the total amount of ferrimagnets. The frequency dependence of the magnetic susceptibility, χ_{fd} and χ_{fd}%, usually used to estimate the absolute and relative content of ultrafine (< 20 nm) SP particles, was calculated as $\chi_{lf} - \chi_{hf}$ and $(\chi_{lf} - \chi_{hf})/\chi_{lf} \times 100\%$, respectively [*Dearing et al., 1996*]. Meanwhile, the anhysteretic remanent magnetization (ARM), which is sensitive to SD particles [*Liu et al., 2004*], was measured in an alternating field of 100 mT with a superimposed 0.05 mT bias field. The χ_{ARM} was calculated by ARM normalized by the bias field. The saturated isothermal remanent magnetization (SIRM) was attained at 1 T with an ASC-10 impulse magnetizer and measured with an AGICO JR6 spinner magnetometer.

3 Results

As illustrated in **Table 1 and Figure 1**, in the two sequences, P_t decreased from 0.85% to 0.07%, while Fe_t increased from 6.3% to 17.7%, which resulted in the wide range of P/Fe from 0.008 to 0.179 (**Figures 1a and 1b**). According to the P/Fe, the profiles could be divided into HP sequences with a high P/Fe (0.037 ~ 0.179) and LP sequences with a low P/Fe (0.008 ~ 0.023). These profiles were labeled according to the mean P/Fe in the following order: HP3 > HP2 > HP1 > LP3 > LP2 > LP1 (**Table 1**). The HP and LP sequences were divided by the P/Fe ratios of 0.025 ~ 0.0275, which were proposed to control the FM particle transformation in solution [*Barrón and Torrent, 2002; Cabello et al., 2009*]. Nevertheless, the two sequences have undergone comparable chemical weathering as indicated by the CIA from 85.2 to 96.5 in the HP sequences and from 87.3 to 99.2 in the LP sequences **(Figure 1b).**

For the iron oxides, the total amount of pedogenic iron oxides estimated by the Fe_d ranging from 4.6% to 10.1% in the HP sequence was only slightly lower than that ranging from 5.7% to 12.7% in the LP sequence (**Figure 1c**) due to the opposite change in Fe_t with Fe_d/Fe_t (**Figures 1a and 1c**). In contrast, the Fe_o and Fe_o/Fe_d ratios in the HP sequence were commonly higher than those in the LP sequence (**Figure 1d**). The Hm change from 0.57% to 5.59% in the HP sequence was also slightly lower than that from 0.56% to 8.3% in the LP sequence, but the Hm/(Hm+Gt) ranging from 0.07 to 0.44 in the HP sequence was similar to that ranging from 0.06 to 0.49 in the LP sequence (**Figure 1e**). In addition, the contents of FM particles indicated by χ_{fd}, χ_{ARM} and SIRM were mostly lower in the HP sequence than in the LP sequence, which agrees with the change trends of Fe_d and Hm. However, the proportions of finer FM particles indicated by χ_{fd}%, χ_{fd}/χ_{ARM}, and ARM/SIRM were significantly higher in the HP sequence than in the LP sequence (**Figures 1f-1h**).To explore the P/Fe effect on the enrichment of iron oxides and related FM particles, the above parameters were plotted versus P/Fe (**Figure 2**). These parameters have demonstrated a common increase in both sequences except that P_t and Fe_o/Fe_d exhibited monotonic deceasing trends as P/Fe decreased.

4 Discussion

4.1 Monotonic increasing crystallinity of iron oxides with decreasing P/Fe

P_t and Fe_t show opposite linear changes along the two sequences (**Figures 2a and 2e**), which indicates that the loss of P is mainly derived from primary P-bearing minerals (mostly apatite) accompanied by the enrichment of immobile iron oxides

with chemical weathering [*Ruttenberg, 2003*]. However, the soils possess lower Fe_t and higher Fe_d/Fe_t in the HP sequence than in the LP sequence, which thus narrows the differences in Fe_d, Hm and Gt between both sequences. This result could be attributed to the more primary Fe carbonates in the LP sequence, which is easier to weather than the primary Fe silicates in dolomite strata [*Veizer and Mackenzie, 2003*]. Meanwhile, the monotonic decrease in Fe_o/Fe_d with P/Fe indicates that the crystallinity of iron oxide increases as P/Fe decreases (**Figure 2g**). This result confirms that the presence of phosphate can impede the aggregation and crystallization of amorphous iron oxide in soil solution [*Gálvez et al., 1999; Barrón and Torrent, 2002*].

4.2 Comparable Hm and Gt competition in high and low P/Fe sequences

In contrast to the monotonic change in amorphous iron oxide along the two sequences, the competition between crystalline Hm and Gt estimated by Hm/(Hm+Gt) changes comparably as the P/Fe is reduced in each sequence (**Figures 2d and 2h**). The highest Hm/(Hm+Gt) often appears in the middle of the profile **(Figure 1e)** and is located at the highest position of the upslope bedside of the valley **(Table 1)**. Considering that the two sequences were sampled with limited horizontal (< 12 km) and vertical space (< 300 m), the climatic difference can be neglected, but the water redistribution along a slope or a profile can still cause significant variations in Hm/(Hm+Gt). The high Hm/(Hm+Gt) in the middle of the upslope profile often correlates with good drainage and low water activity. Conversely, the low Hm/(Hm+Gt) in the downslope profiles, especially in the top and bottom of the

profile, is often accompanied by poor drainage controlled by surface water and groundwater [*Boero and Schwertmann, 1987; Torrent et al., 2010*]. Furthermore, the high organic matter and rapid biological process on the surface could lead to the preferential dissolution of Hm but favor the formation of Gt [*Schwertmann, 1971*].

Nevertheless, Hm/(Hm+Gt) exhibited a corresponding increase with decreasing P/Fe in the two sequences. Previous studies have found that high P/Fe under acidic conditions often favors the formation of Hm rather than Gt, and the effect became more significant with increasing temperature from 25°C to 100°C [*Gálvez et al., 1999*]. In our study, the soil pH variation is limited from 4 to 6, and the mean annual temperature is approximately 15°C. More importantly, Hm/(Hm+Gt) demonstrates comparable increases in both sequences as P/Fe decreases. Therefore, the change in Hm/(Hm+Gt) in this study was likely mainly controlled by a similar climate and pedogenic environment rather than by P/Fe.

4.3 Different magnetic enhancement patterns in high and low P/Fe sequences

In contrast to the comparable change trends of Hm and Gt, the FM particles revealed different change patterns in the two sequences. The FM particles with increasing sizes indicated by χ_{fd}, χ_{ARM} and SIRM exhibited common enrichment at stable accelerations (R^2 = 0.90, 0.89 and 0.91) in the HP sequence but had unstable even rates (R^2 = 0.53, 0.71 and 0.36) in the LP sequence as P/Fe declined (**Figures 3a-3c**). Meanwhile, the relative contents of finer FM particles indicated by χ_{fd}% and ARM/SIRM were both higher in the HP sequence than those in the LP sequence (**Figures 3d and 3f**). However, χ_{fd}/χ_{ARM} changed comparably but in opposite

directions with the decrease in P/Fe. This result suggests that the FM particles accumulated in the HP sequence are commonly finer than those in the LP sequence, but the FM particles around the boundary of the SP and SD particles could have undergone significant growth in the LP sequence.

4.4 Coordination and competition between Hm and FM particles in high and low P/Fe sequences

To evaluate the amount and size distribution of the FM particles accompanying Hm with decreasing P/Fe and avoid the influence of the Hm content difference in both sequences, the magnetic parameters were normalized by Hm and plotted versus P/Fe. As illustrated in **Figures 3g-3i**, the FM particles accompanying Hm indicated by χ_{fd}/Hm, χ_{ARM}/Hm and SIRM/Hm exhibited similar change trends as those of χ_{fd}, χ_{ARM} and SIRM in **Figures 3a-3c**. However, χ_{ARM}/Hm was comparable in both sequences, while χ_{fd}/Hm and SIRM/Hm were higher in the HP sequence and LP sequence. This result suggests that SD particles were enriched comparably with Hm in two sequences, while the finer and coarser FM particles were enriched in the HP and LP sequences, respectively. In addition, the χ_{fd}%/Hm, (χ_{fd}/χ_{ARM})/Hm and (ARM/SIRM)/Hm, which were calculated to trace the relative change in FM in size with the formation of Hm in **Figures 3j-3l**, commonly reveal monotonic decreasing with decreasing P/Fe. This result suggests the coarsening of FM particles that lack the protection of phosphate ligands.

4.5 Mechanism and their significance in paleoclimate reconstruction

Previous experimental studies have found that organic and inorganic ligands play

an important role in modulating the aging product of ferrihydrite (Fh) [*Cabello et al., 2009*]. The proper level of phosphate via specific adsorption or ligand exchange on the surface of Fh can favor the dehydration and rearrangement of Fh to form Hm but inhibit the dissolution of Fh to form Gt [*Barrón et al., 1997; Gálvez et al., 1999; Xu et al., 2017*]. Mgh-like FM particles increasing in size from SP to SD particles were observed as intermediate products [*Barrón et al., 2003; Torrent et al., 2007; Liu et al., 2008; Hu et al., 2013*] due to their higher thermodynamic stability than Hm in nanometers [*Navrotsky et al., 2008*]. As the experiment was conducted in a wide range of P/Fe [*Barrón and Torrent, 2002*], the FM particles were both gradually enriched as P/Fe decreased when the P/Fe was greater than 0.0275 or less than 0.025. The two magnetism enhancement patterns were divided by a dramatic magnetic reduction as the P/Fe decreased from 0.0275 to 0.025. Our study verifies the P/Fe-mediated processes by assuming that the ratio of P/Fe in solid soils determines the ratio of phosphate and Fh dispersed in soil solution. Moreover, the two sequences with comparable changes in Hm and Gt verifies that the ratio of Hm/(Hm+Gt) can be used as a reasonable climatic and environmental indicator independent of parent materials across a large scale.

However, the ratio of P/Fe plays an important role in modulating the FM particles accompanying the formation of Hm. In natural systems, the change in P/Fe in soils and sediments is often controlled by parent material composition and chemical weathering intensity. Carbonates deposited in marine environments often possess a much higher mean P/Fe of approximately 0.170 than that of granites with P/Fe of

293 approximately 0.043 ~ 0.059, although the Fe content in carbonates is much lower
294 than that of granites [*Chen and Wang, 2005*]. Such difference explains the extremely
295 high magnetism of soils in Terra Rossa derived from carbonate [*Grison et al., 2011;*
296 *Lu et al., 2012*] if the regional climate favors the formation of Hm. In addition, the
297 soils derived from basalts that have a high Fe content but a lower P/Fe of
298 approximately 0.010 [*Chen and Wang, 2005*] have high magnetism and frequently
299 observed FM particle growth and transformation into Hm [*Da Costa et al., 1999; Lu*
300 *et al., 2008; Long et al., 2015; Liu et al., 2017*]. The sediments often possess higher
301 variation in P/Fe depending on the depositing environment and chemical weathering
302 intensity. For the aeolian sediments of loess and red clay on the CLP, the P/Fe of loess
303 and palaeosol of approximately 0.031 is commonly higher than that of red clay and
304 palaeosol in extreme stages, such as S5, of approximately 0.019 [*Chen et al., 2001*],
305 which is also divided by the inflection range at approximately 0.0275 ~ 0.025. Since
306 the composition of aeolian sediments is usually homogeneous [*Guo et al., 2002*], the
307 lower P/Fe ratio is correlated with a higher chemical weathering intensity in red clay
308 than in loess. Thus, when the climate changed gradually from the Tertiary to the
309 Quaternary, the magnetic enhancement patterns shifted from low P/Fe to high P/Fe
310 patterns. The pattern shift led to the decoupling of magnetism and redness in the long
311 term, although the magnetism and redness mostly changed in phase in loess or in red
312 clay. In addition, the warmer climate and the longer depositing time could promote
313 more FM particle transformation into Hm [*Barrón and Torrent, 2002; Jiang et al.,*
314 *2018*] in Tertiary red clay than in Quaternary loess, although these factors are

315 expected to exert a gradual influence rather than an abrupt shift in the change in color
316 and magnetism. Additionally, some other inorganic and organic ligands often concur
317 in soils and sediments, which also change with parent material type, chemical
318 weathering intensity and biological recycling and could influence the formation
319 efficiency of Mgh and Hm despite their lower affinity for iron oxides than phosphate
320 [*Cabello et al., 2009*], especially for soils adjacent to rock and ground with high
321 inorganic and organic ligand content. Therefore, the ligand-protected effect usually
322 masked by chemical weathering intensity could better explain the mechanism of
323 different magnetic enhancement patterns in soils and sediments in addition to climate,
324 which is of great significance in soil taxonomy, paleoenvironment reconstruction and
325 spatial exploration.

326 **5 Conclusions**

327 To explore the ligand effect of P/Fe on the formation efficiency of ferrimagnetic
328 Mgh and antiferromagnetic Hm in soils and sediments, we examined two soil Ferrasol
329 sequences with similar climates but contrasting ratios of P/Fe. The FM particles
330 accompanying the formation of Hm stably accelerated in high P/Fe sequences but
331 unstably increased at even rates in low P/Fe sequences. The accumulation of Mgh
332 particles relative to Hm generally became less abundant and coarser under a low P/Fe.
333 This result is attributed to the more rapid grain growth of FM particles and
334 transformation into Hm without enough P ligand protection to retard the
335 crystallization of iron oxides. The ligand-protected effect would help interpret the
336 asynchronous changes in magnetism and redness in soils and sediments controlled by

different enrichment patterns at large spatial and temporal scales, especially in soil taxonomy, paleoclimate reconstruction and spatial exploration.

Acknowledgments

We thank Yunfeng Cai and Dengchun Xing for their help in the laborious field work in mountainous southwestern China. This study was co-supported by the National Natural Science Foundation of China (41877369) and the Natural Science Foundation of Chongqing, China (CSTC2018JCYJAX0456). The original data presented in this paper can be accessed through the public domain repository Zenodo at https://doi.org/10.5281/zenodo.3932444.

346 **Table 1.** Mean values of chemical weathering parameters and iron oxides along different P/Fe profiles

Profile/Sequence	Altitude (m)	P_t (%)	Fe_t (%)	P/Fe	CIA	Fe_d (%)	Fe_o (%)	Hm (%)	Fe_d/Fe_t	Fe_o/Fe_d	Hm/(Hm+Gt)	χ_{lf} (10^{-8} m^3 kg^{-1})
HP3	2010	0.67	10.3	0.118	88.5	7.3	0.39	2.83	0.71	0.05	0.27	244
HP2	2256	0.58	9.6	0.117	91.2	6.6	0.55	2.14	0.67	0.09	0.20	836
HP1	2266	0.26	11.0	0.042	95.4	7.8	0.72	3.52	0.71	0.09	0.33	2140
LP3	1976	0.14	14.2	0.018	90.2	7.6	0.35	2.62	0.53	0.05	0.23	914
LP2	1976	0.12	14.2	0.015	94.5	7.8	0.41	3.82	0.55	0.06	0.33	1345
LP1	2158	0.10	16.7	0.011	97.7	11.2	0.41	6.33	0.67	0.04	0.39	2413
HP sequence	2177	0.51	10.3	0.095	91.6	7.2	0.56	2.76	0.69	0.08	0.26	1050
LP sequence	2037	0.12	15.1	0.015	94.1	9.0	0.39	4.30	0.59	0.05	0.31	1576

347

Figure 1. (a) P_t and Fe_t change in opposite directions along the two sequences. **(b)** P/Fe is commonly higher in the HP sequences than in the LP sequences with comparable chemical weathering indicated by the CIA (chemical alternation index). **(c)** Fe_d is slightly lower in the HP sequence than in the LP sequence due to opposite changes in Fe_t and Fe_d/Fe_t. **(d and e)** Amorphous iron oxides indicated by Fe_o and Fe_o/Fe_d are both higher in the HP sequence, while crystalline iron oxides indicated by Hm and Hm/(Hm+Gt) are slightly higher in the LP sequence. **(f-h)** The absolute magnetic parameters of χ_{lf}, χ_{ARM} and SIRM are slightly lower in the HP sequence, but the relative parameters of χ_{fd}%, χ_{fd}/χ_{ARM} and ARM/SIRM are commonly higher in the HP sequence.

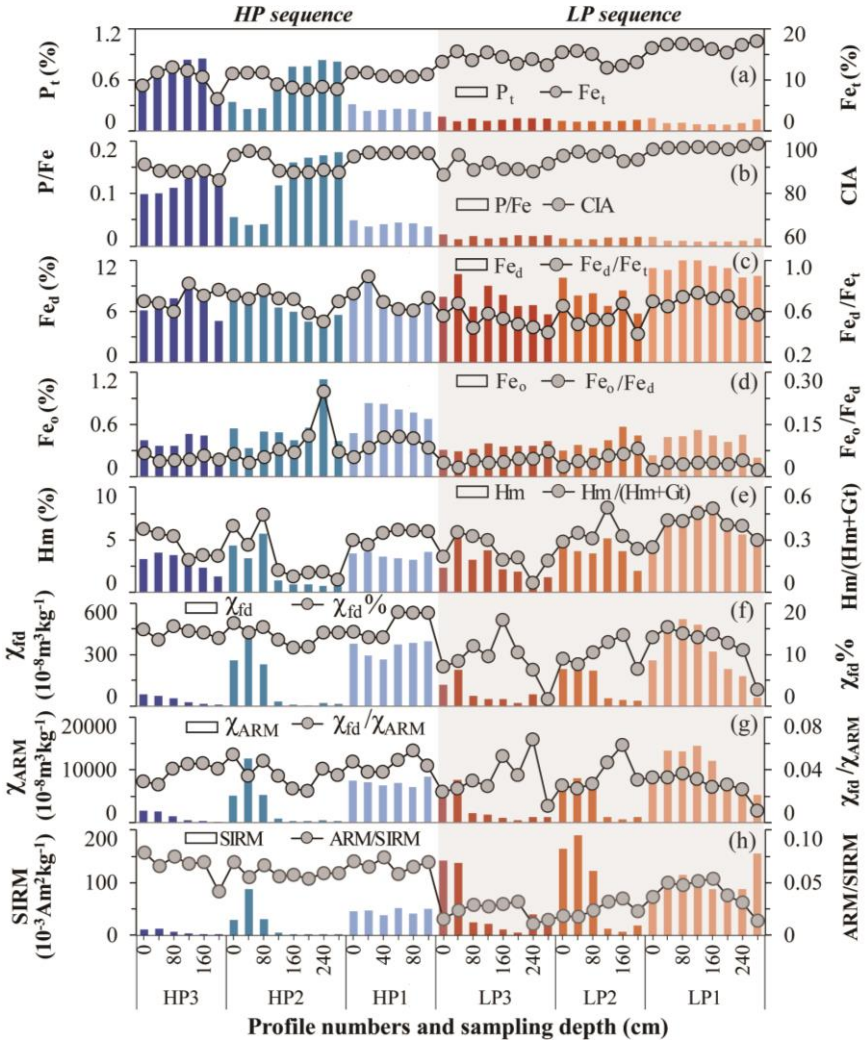
HP sequence
LP sequence
(a)
(b)
(c)
(d)
(e)
(f)
(g)
(h)
HP3
HP2
HP1
LP3
LP2
LP1
Profile numbers and sampling depth (cm)

359

Figure 2. (a and e) P_t and Fe_t monotonously decrease and increase, respectively, with the decease of P/Fe in both sequences. **(b-d, f-h)** The Fe_d, Fe_o, Hm and their ratio parameters increase comparably as P/Fe decreases in two sequences except that the Fe_o/Fe_d decreases monotonically. Note that the x-axis of P/Fe is illustrated in reverse order to indicate chemical weathering intensity from weak to strong. The LP sequence with low P/Fe below 0.025 was shadowed and enlarged independently on the right.

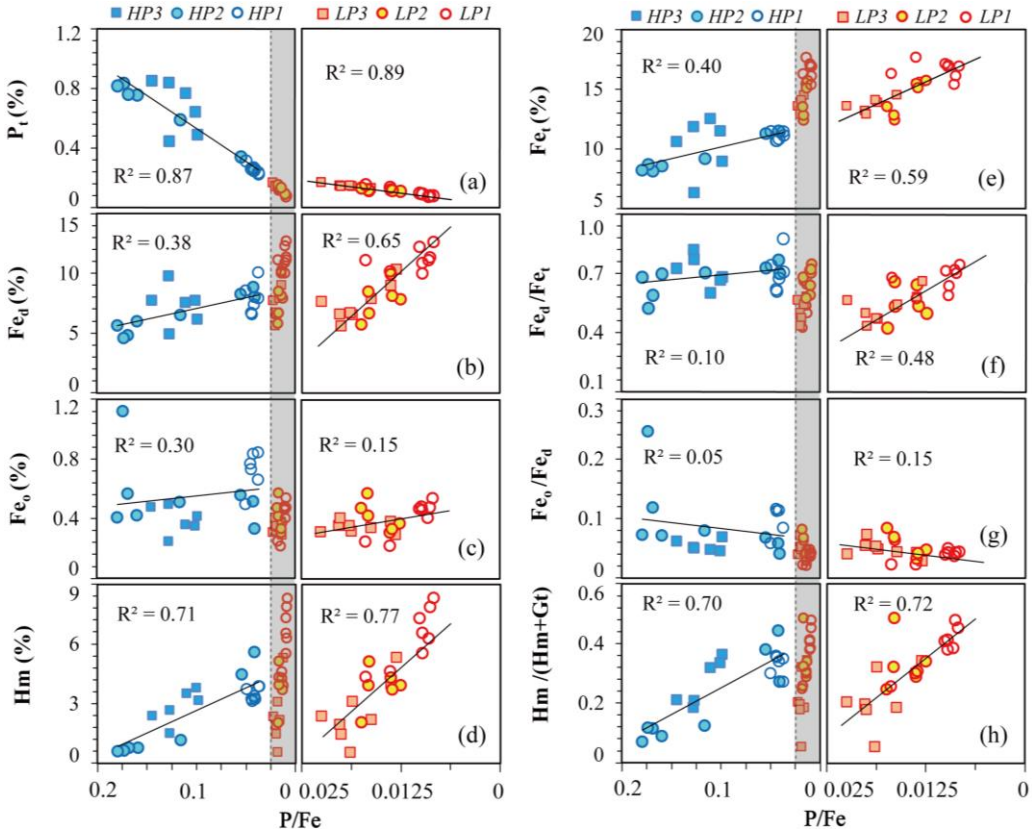

Figure 3. (a-c) Magnetic parameters, including χ_{fd}, χ_{ARM} and SIRM, increase stably and exponentially in the HP sequence but unstably and linearly in the LP sequence with decreasing P/Fe. **(d-f)** The ratios of finer FM particles, including χ_{fd}%, χ_{fd}/χ_{ARM} and ARM/SIRM, change slowly in the HP sequence but rapidly in the LP sequence. **(g-i)** The fine and coarse magnetic particles accompanying the formation of Hm indicated by χ_{fd}/Hm and SIRM/Hm are mostly higher and lower, respectively, in the HP sequence than those in the LP sequence, while the intermediate SD particles remain comparable. **(j-l**) The relative change in the grain size of FM particles accompanying Hm indicated by χ_{fd}%/Hm, (χ_{fd}/χ_{ARM})/Hm and (ARM/SIRM)/Hm decreases monotonically with decreasing P/Fe.

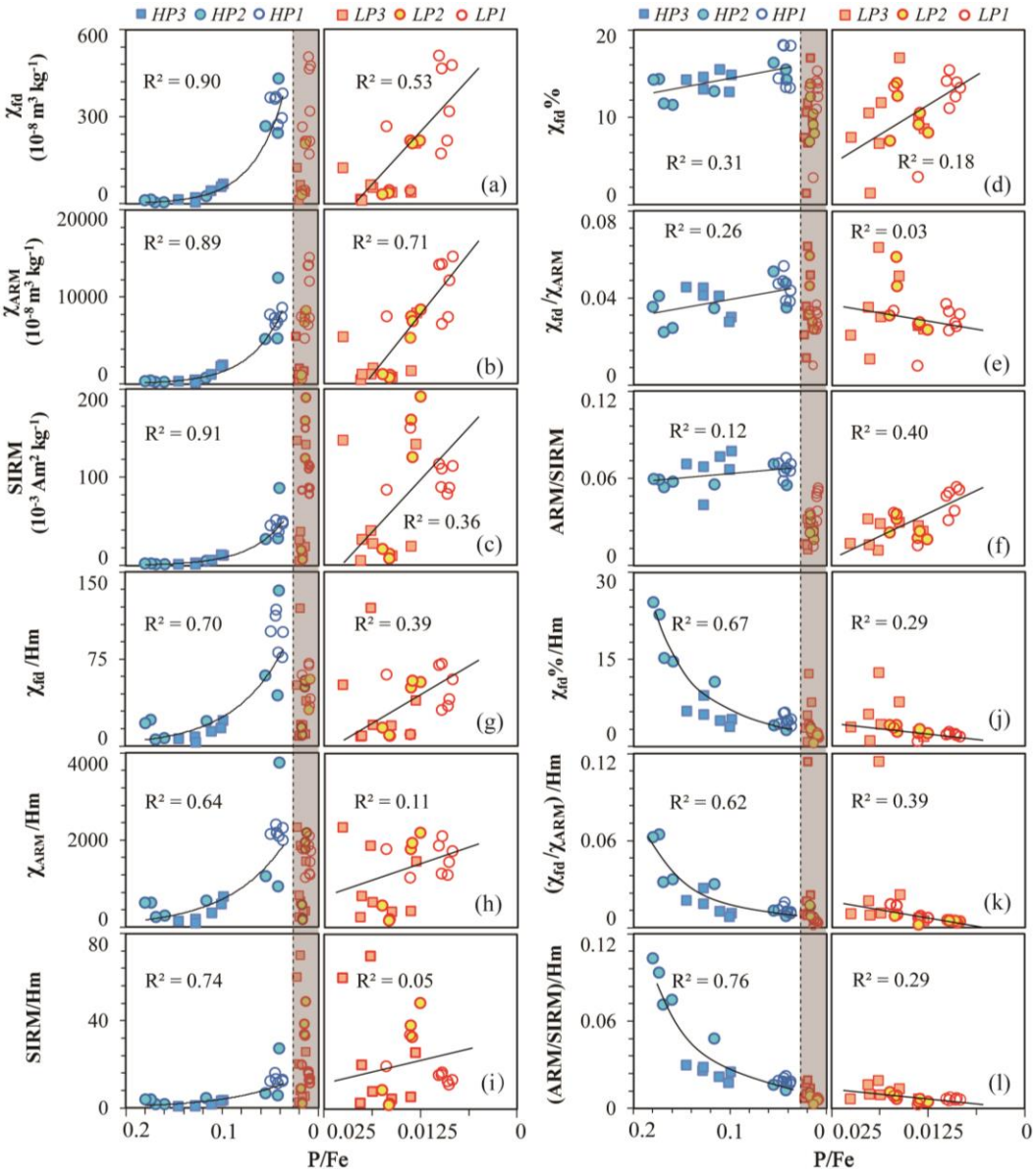
HP3 HP2 HP1 LP3 LP2 LP1
χfd (10-8 m3 kg-1)
R² = 0.90
R² = 0.53
(a)
χARM (10-8 m3 kg-1)
R² = 0.89
R² = 0.71
(b)
SIRM (10-3 Am2 kg-1)
R² = 0.91
R² = 0.36
(c)
χfd /Hm
R² = 0.70
R² = 0.39
(g)
χARM /Hm
R² = 0.64
R² = 0.11
(h)
SIRM/Hm
R² = 0.74
R² = 0.05
(i)
χfd %
R² = 0.31
R² = 0.18
(d)
χfd /χARM
R² = 0.26
R² = 0.03
(e)
ARM/SIRM
R² = 0.12
R² = 0.40
(f)
χfd %/Hm
R² = 0.67
R² = 0.29
(j)
(χfd /χARM) /Hm
R² = 0.62
R² = 0.39
(k)
(ARM/SIRM)/Hm
R² = 0.76
R² = 0.29
(l)
P/Fe
P/Fe

379

References

Balsam, W., J.F. Ji, and J. Chen (2004), Climatic interpretation of the Luochuan and Lingtai loess sections, China, based on changing iron oxide mineralogy and magnetic susceptibility, *Earth and Planetary Science Letters*, *223*(3-4), 335-348. https://doi.org/10.1016/j.epsl.2004.04.023

Barrón, V., N. Gálvez, M.F. Hochella, and J. Torrent (1997), Epitaxial overgrowth of goethite on hematite synthesized in phosphate media: A scanning force and transmission electron microscopy study, *American Mineralogist*, *82*(11-12), 1091-1100. https://doi.org/10.2138/am-1997-11-1206

Barrón, V., and J. Torrent (2002), Evidence for a simple pathway to maghemite in Earth and Mars soils, *Geochimica Et Cosmochimica Acta*, *66*(15), 2801-2806. https://doi.org/10.1016/S0016-7037(02)00876-1

Barrón, V., J. Torrent, and E. de Grave (2003), Hydromaghemite, an intermediate in the hydrothermal transformation of 2-line ferrihydrite into hematite, *American Mineralogist*, *88*(11-12), 1679-1688. https://doi.org/10.2138/am-2003-11-1207

Boero, V., and U. Schwertmann (1987), Occurrence and transformations of iron and manganese in a colluvial Terra Rossa toposequence of Northern Italy, *Catena*, *14*(6), 519-531. https://doi.org/10.1016/0341-8162(87)90003-8

Borggaard, O.K. (1983), The influence of iron-oxides on phosphate adsorption by soil, *Journal of Soil Science*, *34*(2), 333-341. https://doi.org/10.1111/j.1365-2389.1983.tb01039.x

Bortoluzzi, E.C., C.A.S. Perez, J.D. Ardisson, T. Tiecher, and L. Caner (2015), Occurrence of iron and aluminum sesquioxides and their implications for the P sorption in subtropical soils, *Applied Clay Science*, *104*, 196-204. https://doi.org/10.1016/j.clay.2014.11.032

Brenner, J., W. Porter, J.R. Phillips, J. Childs, X.J. Yang, and M.A. Mayes (2019), Phosphorus sorption on tropical soils with relevance to Earth system model needs, *Soil Research*, *57*(1), 17-27. https://doi.org/10.1071/Sr18197

Cabello, E., M.P. Morales, C.J. Serna, V. Barrón, and J. Torrent (2009), Magnetic enhancement during the crystallization of ferrihydrite at 25 and 50 degrees C, *Clays and Clay Minerals*, *57*(1), 46-53. https://doi.org/10.1346/Ccmn.2009.0570105

Chacon, N., W.L. Silver, E.A. Dubinsky, and D.F. Cusack (2006), Iron reduction and soil phosphorus solubilization in humid tropical forests soils: The roles of labile carbon pools and an electron shuttle compound, *Biogeochemistry*, *78*(1), 67-84. https://doi.org/10.1007/s10533-005-2343-3

Chen, J., Z.S. An, L.W. Liu, J.F. Ji, J.D. Yang, and Y. Chen (2001), Variations in chemical compositions of the eolian dust in Chinese Loess Plateau over the past 2.5 Ma and chemical weathering in the Asian inland, *Science in China Series D-Earth Sciences*, *44*(5), 403-413. https://doi.org/10.1007/Bf02909779

Chen, J., and H.N. Wang (2005), Geochemistry, Science Press, Beijing, 418 pp.

Chen, T.H., Q.Q. Xie, H.F. Xu, J. Chen, J.F. Ji, H.Y. Lu, and W. Balsam (2010), Characteristics and formation mechanism of pedogenic hematite in Quaternary

Chinese loess and paleosols, *Catena*, *81*(3), 217-225. https://doi.org/10.1016/j.catena.2010.04.001

Chernyshova, I.V., M.F. Hochella, and A.S. Madden (2007), Size-dependent structural transformations of hematite nanoparticles. 1. Phase transition, *Physical Chemistry Chemical Physics*, *9*(14), 1736-1750. https://doi.org/10.1039/b618790k

Christensen, P.R., R.V. Morris, M.D. Lane, J.L. Bandfield, and M.C. Malin (2001), Global mapping of Martian hematite mineral deposits: Remnants of water-driven processes on early Mars, *Journal of Geophysical Research-Planets*, *106*(E10), 23873-23885. https://doi.org/10.1029/2000je001415

Cornell, R.M., and U. Schwtermann (2003), The Iron Oxides: Structure, Properties, Reactions, Occurrences and Uses, Wiley-VCH Verlag GmbH & Co.KGaA, Weinheim, 661 pp.

Da Costa, A.C.S., J.M. Bigham, F.E. Rhoton, and S.J. Traina (1999), Quantification and characterization of maghemite in soils derived from volcanic rocks in southern Brazil, *Clays and Clay Minerals*, *47*(4), 466-473. https://doi.org/10.1346/Ccmn.1999.0470408

Davey, B.G., J.D. Russell, and M.J. Wilson (1975), Iron-oxide and clay-minerals and their relation to colors of red and yellow podzolic soils near Sydney, Australia, *Geoderma*, *14*(2), 125-138. https://doi.org/10.1016/0016-7061(75)90071-3

Dearing, J.A., R.J.L. Dann, K. Hay, J.A. Lees, P.J. Loveland, B.A. Maher, and K. OGrady (1996), Frequency-dependent susceptibility measurements of environmental materials, *Geophysical Journal-Oxford*, *124*(1), 228-240. https://doi.org/10.1111/j.1365-246X.1996.tb06366.x

Deng, C.L., J. Shaw, Q.S. Liu, Y.X. Pan, and R.X. Zhu (2006), Mineral magnetic variation of the Jingbian loess/paleosol sequence in the northern Loess Plateau of China: Implications for Quaternary development of Asian aridification and cooling, *Earth and Planetary Science Letters*, *241*(1-2), 248-259. https://doi.org/10.1016/j.epsl.2005.10.020

Fang, X.M., C. Garzione, R. Van der Voo, J.J. Li, and M.J. Fan (2003), Flexural subsidence by 29 Ma on the NE edge of Tibet from the magnetostratigraphy of Linxia Basin, China, *Earth and Planetary Science Letters*, *210*(3-4), 545-560. https://doi.org/10.1016/S0012-821x(03)00142-0

Fink, J.R., A.V. Inda, J. Bavaresco, V. Barron, J. Torrent, and C. Bayer (2016), Adsorption and desorption of phosphorus in subtropical soils as affected by management system and mineralogy, *Soil & Tillage Research*, *155*, 62-68. https://doi.org/10.1016/j.still.2015.07.017

Gálvez, N., V. Barrón, and J. Torrent (1999), Effect of phosphate on the crystallization of hematite, goethite, and lepidocrocite from ferrihydrite, *Clays and Clay Minerals*, *47*(3), 304-311. https://doi.org/10.1346/Ccmn.1999.0470306

Gao, X.B., Q.Z. Hao, L. Wang, F. Oldfield, J. Bloemendal, C.L. Deng, Y. Song, J.Y. Ge, H.B. Wu, B. Xu, F.J. Li, L. Han, Y. Fu, and Z.T. Guo (2018), The different climatic response of pedogenic hematite and ferrimagnetic minerals: Evidence

from particle-sized modern soils over the Chinese Loess Plateau, *Quaternary Science Reviews*, *179*, 69-86. https://doi.org/10.1016/j.quascirev.2017.11.011

Grison, H., E. Petrovský, N. Jordanova, and A. Kapička (2011), Strongly magnetic soil developed on a non-magnetic rock basement: A case study from NW Bulgaria, *Studia Geophysica Et Geodaetica*, *55*(4), 697-716. https://doi.org/10.1007/s11200-009-0489-5

Guo, Z.T., W.F. Ruddiman, Q.Z. Hao, H.B. Wu, Y.S. Qiao, R.X. Zhu, S.Z. Peng, J.J. Wei, B.Y. Yuan, and T.S. Liu (2002), Onset of Asian desertification by 22 Myr ago inferred from loess deposits in China, *Nature*, *416*(6877), 159-163. https://doi.org/10.1038/416159a

Gutiérrez, L., V. Barrón, M. Andrés-Vergés, C.J. Serna, S. Veintemillas-Verdaguer, M.P. Morales, and F.J. Lázaro (2016), Detailed magnetic monitoring of the enhanced magnetism of ferrihydrite along its progressive transformation into hematite, *Journal of Geophysical Research-Solid Earth*, *121*(6), 4118-4129. https://doi.org/10.1002/2016jb013016

Han, J.M., H.Y. Lu, N.Q. Wu, and Z.T. Guo (1996), The magnetic susceptibility of modern soils in China and its use for paleoclimate peconstruction, *Studia Geophysica Et Geodaetica*, *40*(3), 262-275. https://doi.org/10.1007/Bf02300742

Hiemstra, T. (2015), Formation, stability, and solubility of metal oxide nanoparticles: Surface entropy, enthalpy, and free energy of ferrihydrite, *Geochimica Et Cosmochimica Acta*, *158*, 179-198. https://doi.org/10.1016/j.gca.2015.02.032

Hu, P.X., Q.S. Liu, J. Torrent, V. Barron, and C.S. Jin (2013), Characterizing and quantifying iron oxides in Chinese loess/paleosols: Implications for pedogenesis, *Earth and Planetary Science Letters*, *369*, 271-283. https://doi.org/10.1016/j.epsl.2013.03.033

Hu, X.F., Y. Du, C.L. Guan, Y. Xue, and G.L. Zhang (2014), Color variations of the Quaternary Red Clay in southern China and its paleoclimatic implications, *Sedimentary Geology*, *303*, 15-25. https://doi.org/10.1016/j.sedgeo.2014.01.006

Ji, J.F., J. Chen, W. Balsam, H.Y. Lu, Y.B. Sun, and H.F. Xu (2004), High resolution hematite/goethite records from Chinese loess sequences for the last glacial-interglacial cycle: Rapid climatic response of the East Asian Monsoon to the tropical Pacific, *Geophysical Research Letters*, *31*(3), L03207. https://doi.org/10.1029/2003gl018975

Jiang, Z.X., Q.S. Liu, A.P. Roberts, V. Barrón, J. Torrent, and Q. Zhang (2018), A new model for transformation of ferrihydrite to hematite in soils and sediments, *Geology*, *46*(11), 987-990. https://doi.org/10.1130/G45386.1

Liu, Q.S., V. Barrón, J. Torrent, S.G. Eeckhout, and C.L. Deng (2008), Magnetism of intermediate hydromaghemite in the transformation of 2-line ferrihydrite into hematite and its paleoenvironmental implications, *Journal of Geophysical Research-Solid Earth*, *113*(B1), B01103. https://doi.org/10.1029/2007jb005207

Liu, Q.S., J. Bloemendal, J. Torrent, and C.L. Deng (2006), Contrasting behavior of

hematite and goethite within paleosol S5 of the Luochuan profile, Chinese Loess Plateau, *Geophysical Research Letters*, *33*(20), L20301. https://doi.org/10.1029/2006gl027172

Liu, Q.S., M.J. Jackson, Y.J. Yu, F.H. Chen, C.L. Deng, and R.X. Zhu (2004), Grain size distribution of pedogenic magnetic particles in Chinese loess/paleosols, *Geophysical Research Letters*, *31*(22), L22603. https://doi.org/10.1029/2004gl021090

Liu, Q.S., A.P. Roberts, J.C. Larrasoana, S.K. Banerjee, Y. Guyodo, L. Tauxe, and F. Oldfield (2012), Environmental magnetism: principles and applications, *Reviews of Geophysics*, *50*, RG4002. https://doi.org/10.1029/2012rg000393

Liu, X.M., T. Rolph, Z.S. An, and P. Hesse (2003), Paleoclimatic significance of magnetic properties on the Red Clay underlying the loess and paleosols in China, *Palaeogeography Palaeoclimatology Palaeoecology*, *199*(1-2), 153-166. https://doi.org/10.1016/S0031-0182(03)00504-2

Liu, Z.F., Q.S. Liu, J. Torrent, V. Barrón, and P.X. Hu (2013), Testing the magnetic proxy χ_{FD}/HIRM for quantifying paleoprecipitation in modern soil profiles from Shaanxi Province, China, *Global and Planetary Change*, *110*, 368-378. https://doi.org/10.1016/j.gloplacha.2013.04.013

Liu, Z.F., J.L. Ma, G.J. Wei, Q.S. Liu, Z.X. Jiang, X. Ding, S.S. Peng, T. Zeng, and T.P. Ouyang (2017), Magnetism of a red soil core derived from basalt, northern Hainan Island, China: Volcanic ash versus pedogenesis, *Journal of Geophysical Research-Solid Earth*, *122*(3), 1677-1696. https://doi.org/10.1002/2016jb013834

Long, X.Y., J.F. Ji, and W. Balsam (2011), Rainfall-dependent transformations of iron oxides in a tropical saprolite transect of Hainan Island, South China: Spectral and magnetic measurements, *Journal of Geophysical Research-Earth Surface*, *116*, F03015. https://doi.org/10.1029/2010jf001712

Long, X.Y., J.F. Ji, W. Balsam, V. Barrón, and J. Torrent (2015), Grain growth and transformation of pedogenic magnetic particles in red Ferralsols, *Geophysical Research Letters*, *42*(14), 5762-5770. https://doi.org/10.1002/2015gl064678

Long, X.Y., J.F. Ji, V. Barrón, and J. Torrent (2016), Climatic thresholds for pedogenic iron oxides under aerobic conditions: Processes and their significance in paleoclimate reconstruction, *Quaternary Science Reviews*, *150*, 264-277. https://doi.org/10.1016/j.quascirev.2016.08.031

Lovley, D.R., and E.J.P. Phillips (1986), Organic-matter mineralization with reduction of ferric iron in anaerobic sediments, *Applied and Environmental Microbiology*, *51*(4), 683-689. https://doi.org/10.1128/Aem.51.4.683-689.1986

Lu, S.G., D.J. Chen, S.Y. Wang, and Y.D. Liu (2012), Rock magnetism investigation of highly magnetic soil developed on calcareous rock in Yun-Gui Plateau, China: Evidence for pedogenic magnetic minerals, *Journal of Applied Geophysics*, *77*, 39-50. https://doi.org/10.1016/j.jappgeo.2011.11.008

Lu, S.G., Q.F. Xue, L. Zhu, and J.Y. Yu (2008), Mineral magnetic properties of a weathering sequence of soils derived from basalt in Eastern China, *Catena*, *73*(1), 23-33. https://doi.org/10.1016/j.catena.2007.08.004

Mullins, C.E. (1977), Magnetic-susceptibility of soil and its significance in soil science - review, *Journal of Soil Science*, *28*(2), 223-246. https://doi.org/10.1111/j.1365-2389.1977.tb02232.x

Navrotsky, A., L. Mazeina, and J. Majzlan (2008), Size-driven structural and thermodynamic complexity in iron oxides, *Science*, *319*(5870), 1635-1638. https://doi.org/10.1126/science.1148614

Nie, J.S., Y.G. Song, and J.W. King (2016), A review of recent advances in Red-Clay environmental magnetism and paleoclimate history on the Chinese Loess Plateau, *Frontiers in Earth Science*, *4*. https://doi.org/10.3389/feart.2016.00027

Nie, J.S., Y.G. Song, J.W. King, X.M. Fang, and C. Heil (2010), HIRM variations in the Chinese red-clay sequence: Insights into pedogenesis in the dust source area, *Journal of Asian Earth Sciences*, *38*(3-4), 96-104. https://doi.org/10.1016/j.jseaes.2009.11.002

Poggere, G.C., V. Barron, A.V. Inda, J.Z. Barbosa, A.D.B. Brito, and N. Curi (2020), Linking phosphorus sorption and magnetic susceptibility in clays and tropical soils, *Soil Research*, *58*(5), 430-440 https://doi.org/10.1071/Sr20099

Ruttenberg, K.C. (2003), The global phosphorus cycle, Treatise on Geochemistry 8, Elsevier Inc 585-643 pp.

Schwertmann, U. (1971), Transformation of hematite to goethite in soils, *Nature*, *232*(5313), 624-625. https://doi.org/10.1038/232624a0

Taylor, R.M., and U. Schwertmann (1974), Association of phosphorus with iron in ferruginous soil concretions, *Australian Journal of Soil Research*, *12*(2), 133-145. https://doi.org/10.1071/Sr9740133

Torrent, J., V. Barrón, and Q.S. Liu (2006), Magnetic enhancement is linked to and precedes hematite formation in aerobic soil, *Geophysical Research Letters*, *33*(2), L02401. https://doi.org/10.1029/2005gl024818

Torrent, J., Q.S. Liu, and V. Barrón (2010), Magnetic susceptibility changes in relation to pedogenesis in a Xeralf chronosequence in northwestern Spain, *European Journal of Soil Science*, *61*(2), 161-173. https://doi.org/10.1111/j.1365-2389.2009.01216.x

Torrent, J., Q.S. Liu, J. Bloemendal, and V. Barrón (2007), Magnetic enhancement and iron oxides in the upper luochuan Loess-paleosol sequence, Chinese Loess plateau, *Soil Science Society of America Journal*, *71*(5), 1570-1578. https://doi.org/10.2136/sssaj2006.0328

Veizer, J., and F.T. Mackenzie (2003), Evolution of Sedimentary Rocks, Treatise on Geochemistry 7, 369-407 pp.

Vilar, C.C., A.C.S. da Costa, A. Hoepers, and I.G. de Souza (2010), Maximum phosphorus adsorption capacity as related to iron and aluminum forms in subtropical soils, *Revista Brasileira De Ciencia Do Solo*, *34*(4), 1059-1068. https://doi.org/10.1590/S0100-06832010000400006

Wang, L.J., C.V. Putnis, J. Hovelmann, and A. Putnis (2018), Interfacial precipitation of phosphate on hematite and goethite, *Minerals*, *8*(5), 207. https://doi.org/10.3390/min8050207

Wang, X.M., Y.F. Hu, Y.D. Tang, P. Yang, X.H. Feng, W.Q. Xu, and M.Q. Zhu (2017), Phosphate and phytate adsorption and precipitation on ferrihydrite surfaces, *Environmental Science-Nano*, *4*(11), 2193-2204. https://doi.org/10.1039/c7en00705a

Xiao, Z., G.F. Chen, J.T. Pang, and H.R. Yu (2019), Analysis of occurrence state of Cr in phosphate rock of Kunyang Phosphate Mine, *Industrial Minerals & Processing*, *48*(7), 36-39. https://doi.org/10.16283/j.cnki.hgkwyjg

Xiong, Y., and Q.K. Li (1987), Soil in China, Science Press, Beijing, 746 pp.

Xu, C.Y., R.K. Xu, J.Y. Li, and K.Y. Deng (2017), Phosphate-induced aggregation kinetics of hematite and goethite nanoparticles, *Journal of Soils and Sediments*, *17*(2), 352-363. https://doi.org/10.1007/s11368-016-1550-y

Yang, S.L., X.M. Fang, J.J. Li, Z.S. An, S.Y. Chen, and H. Fukusawa (2001), Transformation functions of soil color and climate, *Science in China Series D-Earth Sciences*, *44*, 218-226. https://doi.org/10.1007/Bf02911990

Yin, A (2010), Cenozoic tectonic evolution of Asia: A preliminary synthesis, *Tectonophysics*, *488*(1-4), 293-325. https://doi.org/10.1016/j.tecto.2009.06.002

Zhao, Z.J., R. Jin, D. Fang, H. Wang, Y. Dong, R.K. Xu, and J. Jiang (2018), Paddy cultivation significantly alters the forms and contents of Fe oxides in an Oxisol and increases phosphate mobility, *Soil & Tillage Research*, *184*, 176-180. https://doi.org/10.1016/j.still.2018.07.012

Figure 1.

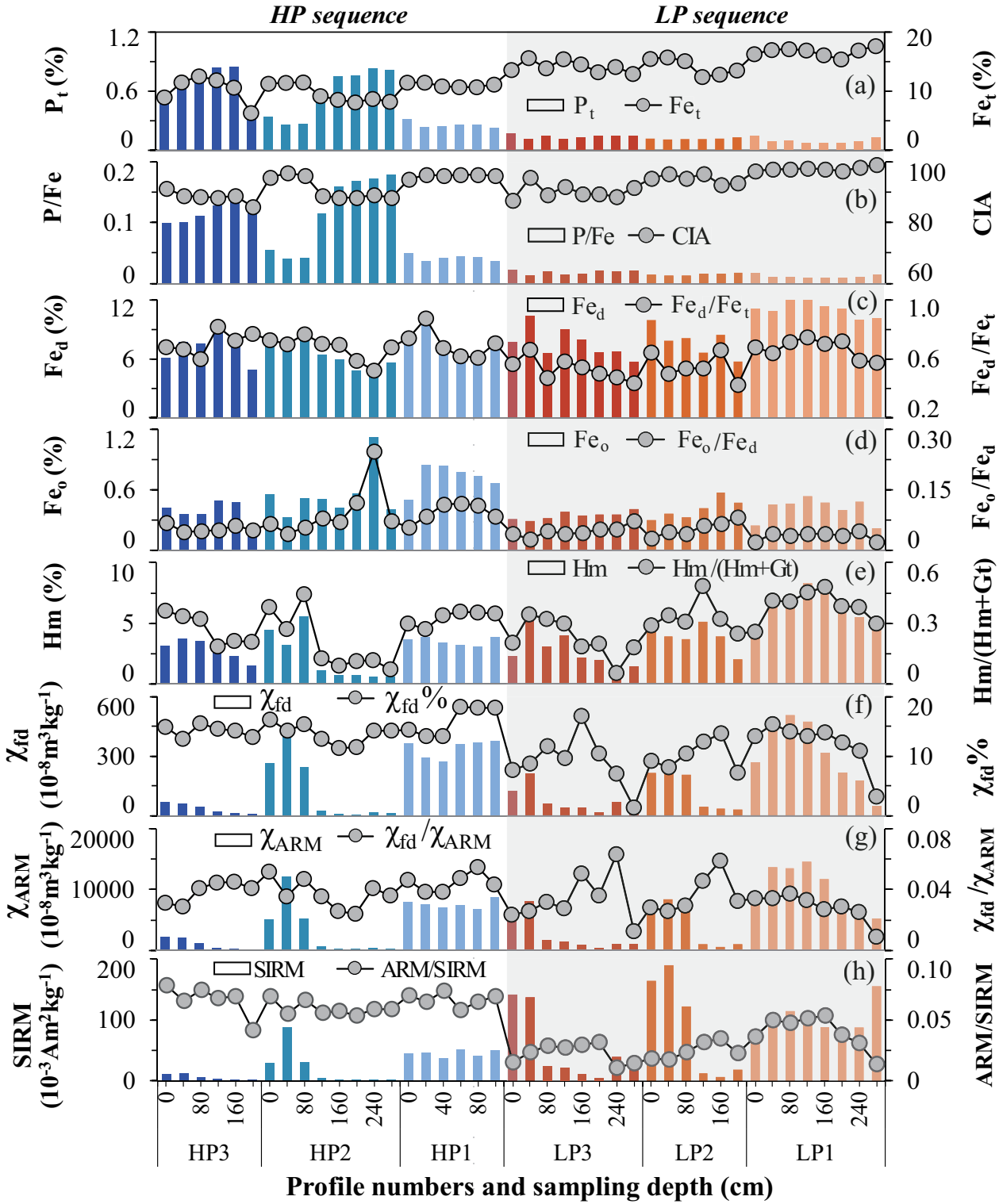
HP sequence
LP sequence
(a)
(b)
(c)
(d)
(e)
(f)
(g)
(h)
P_t (%)
Fe_t (%)
P/Fe
CIA
Fe_d (%)
Fe_d/Fe_t
Fe_o (%)
Fe_o/Fe_d
Hm (%)
Hm/(Hm+Gt)
χfd (10^-8 m^3 kg^-1)
χfd %
χARM (10^-8 m^3 kg^-1)
χfd /χARM
SIRM (10^-3 Am^2 kg^-1)
ARM/SIRM
HP3
HP2
HP1
LP3
LP2
LP1
Profile numbers and sampling depth (cm)

Figure 2.

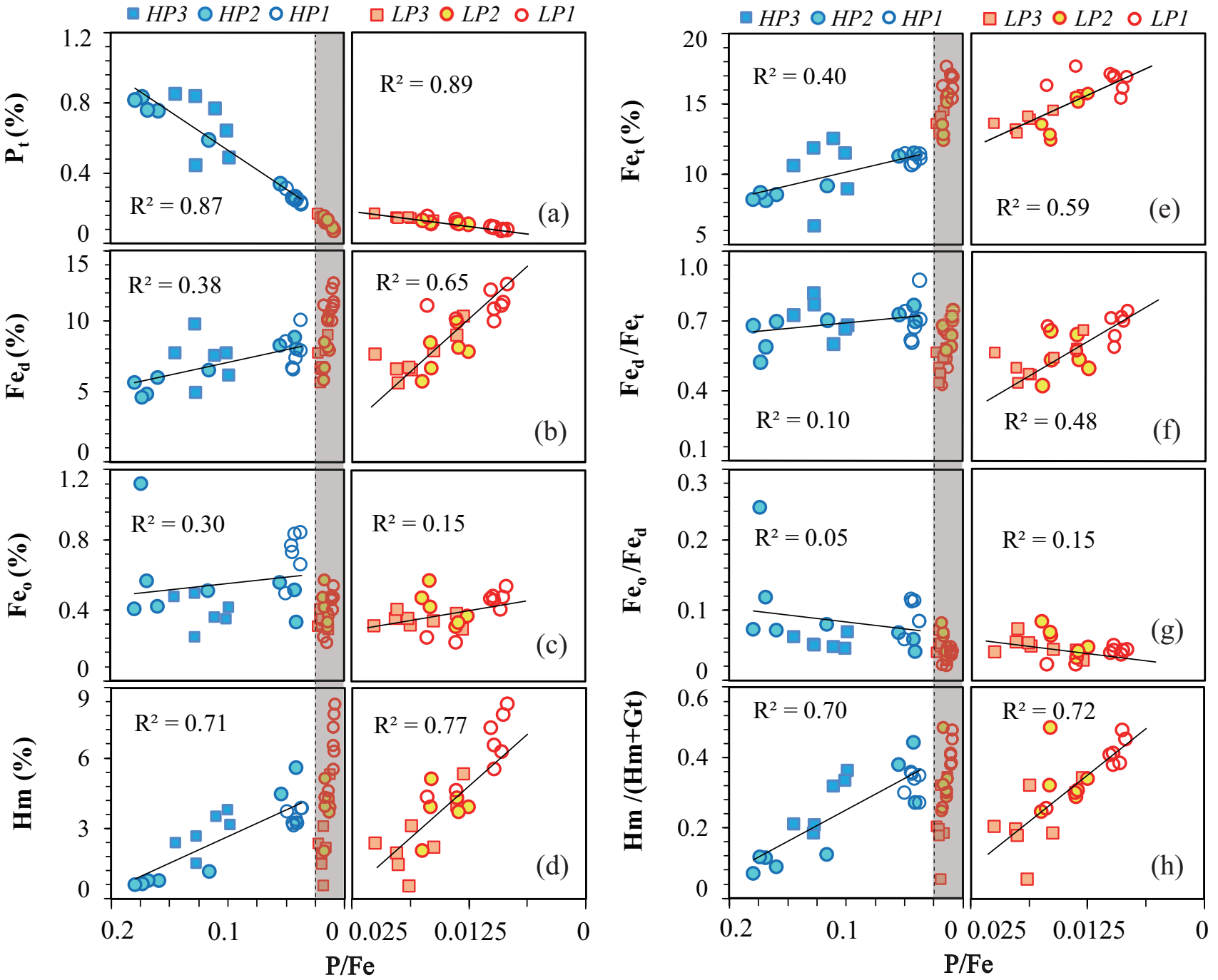
HP3 HP2 HP1 LP3 LP2 LP1
P_t (%)
R² = 0.87
R² = 0.89
(a)
Fe_d (%)
R² = 0.38
R² = 0.65
(b)
Fe_o (%)
R² = 0.30
R² = 0.15
(c)
Hm (%)
R² = 0.71
R² = 0.77
(d)
Fe_t (%)
R² = 0.40
R² = 0.59
(e)
Fe_d/Fe_t
R² = 0.10
R² = 0.48
(f)
Fe_o/Fe_d
R² = 0.05
R² = 0.15
(g)
Hm /(Hm+Gt)
R² = 0.70
R² = 0.72
(h)
P/Fe

Figure 3.

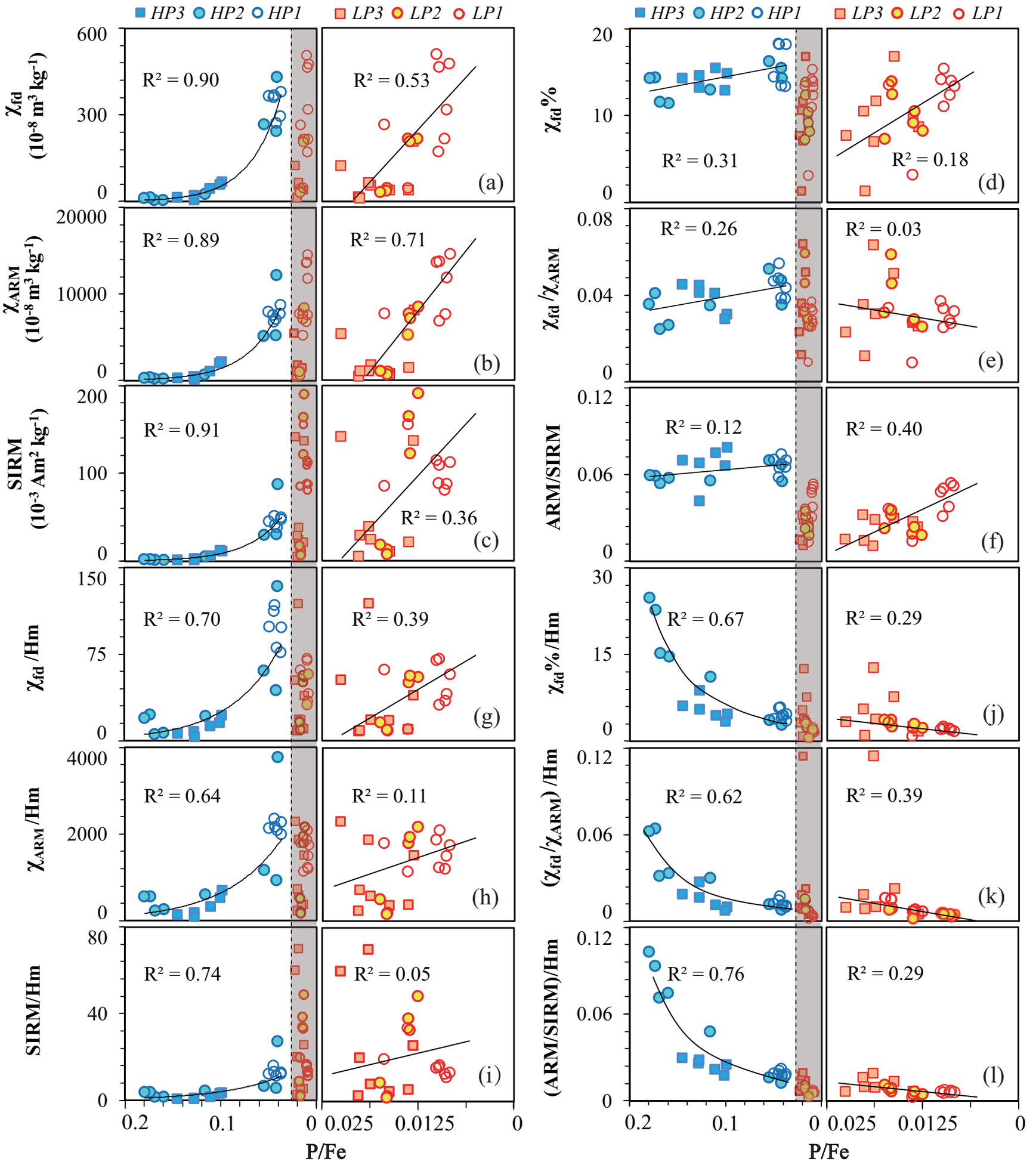
HP3 HP2 HP1 LP3 LP2 LP1
χfd (10-8 m3 kg-1)
R² = 0.90
R² = 0.53
(a)
χARM (10-8 m3 kg-1)
R² = 0.89
R² = 0.71
(b)
SIRM (10-3 Am2 kg-1)
R² = 0.91
R² = 0.36
(c)
χfd /Hm
R² = 0.70
R² = 0.39
(g)
χARM /Hm
R² = 0.64
R² = 0.11
(h)
SIRM/Hm
R² = 0.74
R² = 0.05
(i)
χfd %
R² = 0.31
R² = 0.18
(d)
χfd /χARM
R² = 0.26
R² = 0.03
(e)
ARM/SIRM
R² = 0.12
R² = 0.40
(f)
χfd %/Hm
R² = 0.67
R² = 0.29
(j)
(χfd /χARM) /Hm
R² = 0.62
R² = 0.39
(k)
(ARM/SIRM)/Hm
R² = 0.76
R² = 0.29
(l)
0.2 0.1 0 0.025 0.0125 0
P/Fe